International Journal of Hydrogen Energy 54 (2024) 1120–1129

Contents lists available at ScienceDirect

International Journal of Hydrogen Energy

journal homepage: www.elsevier.com/locate/he

Performance of biogas blended with hydrogen in a commercial self-aspirating burner

Adam J. Gee [a,*], Neil Smith [b], Alfonso Chinnici [a], Paul R. Medwell [a]

[a] School of Electrical and Mechanical Engineering, The University of Adelaide, Adelaide, SA 5005, Australia
[b] School of Chemical Engineering and Advanced Materials, The University of Adelaide, Adelaide, SA 5005, Australia

ARTICLE INFO

Handling Editor: Dr S Nanda

Keywords:
Biogas
Hydrogen
Commercial
Self-aspirating
Heating

ABSTRACT

A natural gas and carbon dioxide fuel mixture was enriched by hydrogen to experimentally measure the performance of a hydrogen and surrogate biogas fuel. The performance of various biogas qualities and hydrogen blend ratios was investigated for use in a commercial self-aspirating burner by quantifying the impact on primary air entrainment, blow-off and flashback limits, NOx emissions, radiant heat transfer and flame appearance. The results showed operating limits of a biogas or hydrogen flame alone could be extended by blending one with the other and by increasing fuel injector size (lowering primary air entrainment), with the latter being more effective. The collateral impact of carbon dioxide and hydrogen addition on radiant heat transfer could be mitigated by increasing injector size, with the carbon dioxide content in biogas maintaining NOx levels at or below the level of natural gas. Overall, there appears to be merit for hydrogen and biogas to operate as a mutually beneficial fuel in a commercial self-aspirating burner design.

1. Introduction

The need for alternative sources of energy continues to grow as the climate situation worsens and fossil fuel reserves are depleted. For many heating applications which currently utilise combustion, switching to electricity may not be a viable decarbonisation approach. For these combustion applications, many have begun to investigate hydrogen (H_2) as an alternative fuel.

Combustion of H_2 produces no carbon dioxide (CO_2) emissions, it can be produced using a variety of methods, including renewable pathways such as electrolysis of water. This method allows for H_2 to be used as an energy storage medium for electricity generated from renewable sources such as wind or solar. The combustion properties of H_2 are distinct from many current fuels and so provide unique opportunities and challenges for sectors looking to use H_2 in their existing burners. Quantifying the magnitude by which these challenges will impact different applications and ultimately de-risking the adoption of H_2 for a range of combustion applications is a critical first step towards decarbonisation.

In addition to H_2, biogas is also a strong contender to replace non-renewable fossil fuels. Biogas refers to the gas mixture produced from the anaerobic digestion of bio-waste and is therefore a renewable and potentially carbon-neutral fuel alternative [1]. The primary feedstock for biogas in these regions come from crop residuals, animal manure and municipal solid waste. Many industries have the potential to produce biogas as a by-product of their normal operations with anaerobic digesters. Europe is the largest producer of biogas in the world, followed by the US and China, who collectively account for 90 % of the world's biogas production [2].

The composition of biogas depends on the feedstock and biodigester conditions, but a typical analysis contains 40–80 % CH_4 with the balance CO_2, and low concentrations of other species such as CO, N_2, H_2, O_2, H_2S, H_2O, dust and siloxanes also present [2–6]. The high concentration of inert CO_2 can make use of biogas for combustion challenging as it dilutes the fuel and limits the combustion process. Separation of the fuel from these inert species adds to the cost of production [1].

The challenges of biogas combustion primarily are a result of its low volumetric energy density, low flame speed and narrow flammability limits due to the high concentration of inert species [6–9]. These challenges make utilisation of raw biogas in commercial burner designs difficult. In fact, raw biogas is often reported as ineligible for use in commercial burners — the low volumetric energy density, as a result of the high inert content, means a considerable increase in total volumetric fuel flow is required to maintain heat input. This, combined with the low burning velocity, result in either much lower heat inputs or extinction

* Corresponding author.
E-mail address: adam.gee@adelaide.edu.au (A.J. Gee).

https://doi.org/10.1016/j.ijhydene.2023.11.322
Received 4 October 2023; Received in revised form 15 November 2023; Accepted 27 November 2023
Available online 3 December 2023

due to blow-off when using biogas [6,10].

Considerable effort is being made to improve the upstream production quality of biogas by optimising digestion techniques [11–13]. From a downstream, end-user perspective, one approach to improve the burning velocity and flammability limits of biogas flames for heating applications, is the blending with H_2 [10,14–20]. The high flame speed and wide flammability limits of H_2 may improve the properties of biogas and make it useable in a variety of commercial heating applications. From an alternative perspective, the high inert content of raw biogas may be an opportunity to address the challenges associated with H_2 combustion. The inert content of biogas may contribute to lowering the high NOx emissions from H_2-blended flames and the (renewable) CO_2 source may also improve the radiant heat transfer properties of the flame [21].

To study the effects of H_2-enrichment of biogas, a CH_4–CO_2 gas mixture can be used to simulate the properties of raw biogas [19,20,22–24]. Investigations of biogas flames under a variety of configurations have shown significant impacts on stability, flame temperature, flame length and heat transfer properties as a result of H_2 addition as low as 5–10 vol% [10,19,20]. Interestingly, it was shown that H_2 addition had a diminishing effect, that is, from 0 % to 5 vol% H_2 had a greater relative impact than from 5 % to 10 vol% H_2 with regard to increasing the upper limit of fuel velocity before critical instability occurred [10,19,20,22]. Characteristic reductions in flame length and radiant heat transfer were also observed in both the premixed and non-premixed cases [10,19]. The influence of H_2 to the non-premixed case caused a reduction in heat transfer, whereas H_2 addition to the premixed case enhanced heat transfer [10,19]. In the self-aspirating case [20], H_2 fraction is considered up to 50 vol% with the aforementioned trends still observed. For fully- and partially-premixed flames, equivalence ratio (φ) contributes significantly to overall performance. In a study of H_2 addition to a biogas surrogate mixture, it was shown that changes in equivalence ratio can have significant effects on heat release, especially under rich ($\varphi = 1.2$) conditions [25]. These effects were improved with the presence of H_2 but worsened by the presence of CO_2 due to physical, chemical and thermal effects.

An important consideration when investigating alternative fuels for industrial use is the collateral effects on heat transfer. Inert dilution has been shown previously to impact the radiant heat transfer properties of flames [26–28]. The displacement of soot as a result of H_2 blending is beneficial from a health and environmental perspective but can be detrimental to the performance of some combustion applications. Blackbody radiation from soot particles contributes the majority of radiative heat transfer and is responsible for the colour and luminosity of non-premixed hydrocarbon flames [21,29–34]. In addition to the reducing effects of H_2 on soot loading, CO_2 has been numerically shown to decrease the soot formation of laminar hydrocarbon diffusion flames via chemical, thermal and dilution pathways [35,36]. In fact, although H_2 and CO_2 both reduced soot formation to a similar degree, albeit via different pathways (H_2 suppressed the soot inception and CO_2 supressed the HACA surface growth pathway), the combination of CO_2 and H_2 was shown to be significantly more effective at lowering soot formation than either added alone, reducing total soot inception by almost 40 % for addition/dilution ratios of 30 % each [35].

It is worth noting that although H_2 has a higher specific energy density than biogas, H_2 still has a relatively low volumetric energy density. Thus, to maintain heat input with a mixture of H_2 or biogas, an increase in total volumetric flow of fuel is required. In diffusion biogas flames, it has been shown that increasing the fuel nozzle size improved the blow-off limit via a decrease in axial velocity [22]. In self-aspirating burners, the added volumetric flow rate provides a unique challenge where the momentum of the fuel stream dictates the amount of primary air entrainment and resulting equivalence ratio inside the burner.

In a self-aspirating burner design it has been shown that blending H_2, while conserving heat input, increases the entrainment of primary air which can lead to flashback and/or performance issues [37]. It was found that increasing the fuel injector size lowered the momentum of the fuel stream and resulting primary air entrainment, and was an effective approach to permit larger fractions of H_2 to be blended without flashback [37]. The drawback to increasing the fuel injector size and lowering primary air intake was found to be reduced performance, primarily in the form of increased NOx emissions [37]. There is potential for these NOx emissions to be partially mitigated by diluting the fuel with an inert species such as CO_2. To make this process more cost-effective, the source of the CO_2 could come from raw biogas. Furthermore, the increased reduced fuel stream velocity induced by a larger fuel injector size, and higher burning velocity of H_2 may extend the blow-off limit of a low-quality biogas (i.e. one which contains high amounts of CO_2). The multi-variable issue of CO_2 dilution, H_2 combustion and the increased primary air entrainment has not been thoroughly investigated with respect to industry-relevant performance criteria.

Although some insight can be drawn from existing literature, there remain several gaps in understanding with regards to the operability and performance of biogas blended with H_2 in commercial burner designs, particularly, in partially-premixed self-aspirating designs. The modification of the fuel injector in a self-aspiring design, which has shown previous success extending the flashback limit for operation with H_2, has potential as a solution for H_2-biogas mixtures. Additionally, the performance of a H_2-biogas mixture has not been investigated in the context of a modified self-aspirating burner. It is therefore necessary to better understand how H_2 addition to biogas of various qualities (CO_2 concentrations) will impact blow-off and flashback behaviour, NOx emissions, radiant heat transfer and flame appearance in a self-aspirating burner design.

This paper compares the performance of a commercial self-aspirating burner operating with H_2-biogas fuel blends compared to its typical operation on natural gas and its operation on H_2-natural gas blends, characterised in previous work [37]. A significant novelty of this work is the detailed characterisation of a commercial burner design using industry-relevant performance metrics. The upper and lower limits of H_2 addition before flashback or blow-off are quantified for a range of biogas compositions. The efficacy of increasing fuel injector size, as a simple and cost-effective means of lowering fuel stream velocity and primary air entrainment is also considered for its ability to extend these limits and its impact on overall performance. The practical performance of the burner is characterised using the criteria: flame appearance (visibility and length), radiant heat transfer and NOx emissions. The work presented in this paper goes beyond previous investigations by considering not just the minimum fraction of H_2 required to achieve stable combustion, but the maximum permissible fraction H_2 before flashback, in addition to several intermediate cases — all of which have been characterised using the above-mentioned performance criteria. Overall, an analysis is provided which describes the ability of a commercial burner design to be adapted to operate effectively on various H_2-biogas blends.

2. Methods

2.1. Burner apparatus

The experimental results presented in this paper were conducted on a commercial self-aspirating burner known as an atmospheric nozzle (AN) burner. Fuel is supplied via a central injector jet with enough momentum such that surrounding atmospheric air can be entrained as primary air. A diagram of the burner is presented in Fig. 1, modified from a previous investigation [37]. The rate of primary air entrainment is a function of the fuel stream momentum (M), which is calculated from the density (ρ) and velocity (U) of the fuel stream, as in Eq (1) [37–39].

$$M = \rho U^2 \tag{1}$$

In addition to the base 4-mm-diameter fuel injector, two addition sizes were investigated, an 8- and 12-mm-diameter. The larger injector size

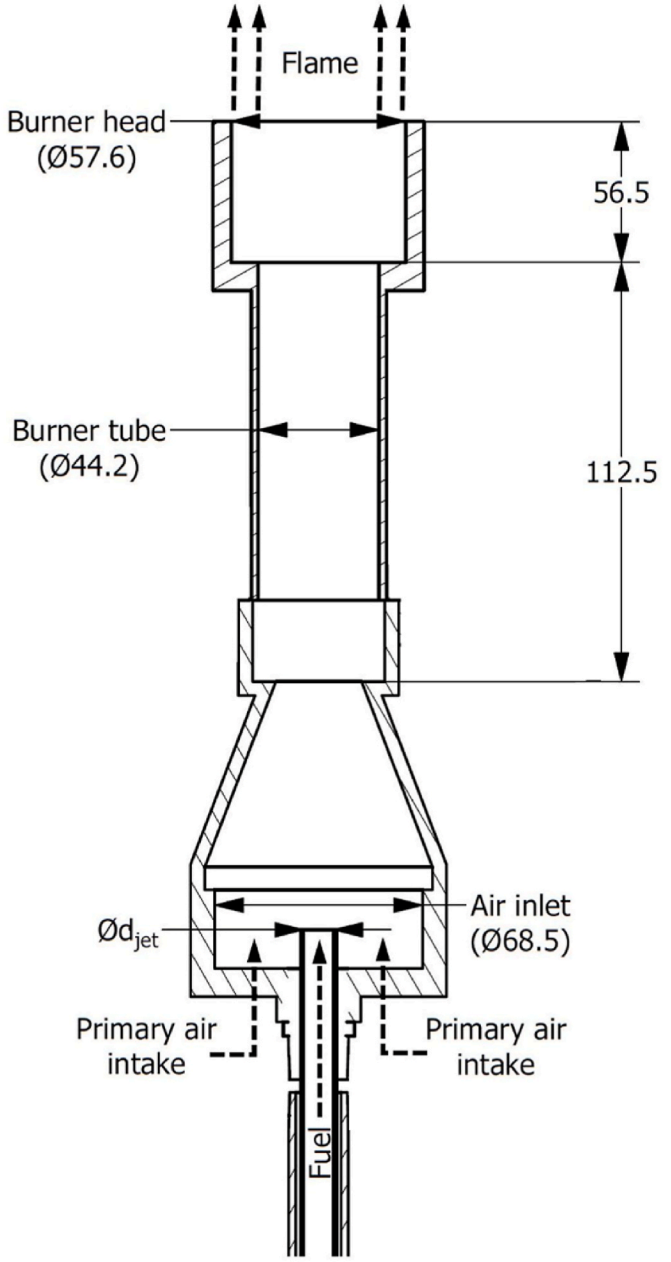

Fig. 1. Burner diagram, adapted from previous work [37], showing major components and their sizes in millimetres. The fuel injector jet size (d_{jet}) was varied from 4 mm to 8 mm or 12 mm. Fuel is issued via the central jet and primary air is entrained from the surroundings via the open-walled design of the venturi inlet.

lowers the fuel stream velocity and, according to Eq (1), the fuel stream momentum. The resulting lower axial momentum and reduced entrainment of primary air was investigated as a means of improving performance and operating limits of the AN-burner on H_2-biogas fuel blends by lowering the fuel stream velocity and increasing equivalence ratio to increase the window of operation between blow-off and flashback.

The volume of primary air entrained for a given fuel blend or injector size was estimated using a predictive model [40,41], presented in Eq (2). The model has been shown previously to be a good predictor of primary air entrainment in self-aspirating designs [37]. Where the ratio of entrained air to fuel (Ψ) was calculated using fuel (ρ_{fuel}) and air (ρ_{air}) density, inner annulus area (A_1), given by the fuel injector geometry (4-, 8- or 12-mm-diameter), and outer annulus area (A_2), given by the venturi air inlet geometry (68.5-mm-diameter)

$$\Psi = \sqrt{\frac{\rho_{fuel}}{\rho_{air}}}\left(\sqrt{\frac{A_2}{A_1}} - 1\right) \tag{2}$$

2.2. Experimental diagnostics

The diagnostic techniques selected for this investigation were chosen to provide a global characterisation of the burner and various fuel blends. In particular, visual and OH* chemiluminescence imaging, axial heat flux and emission measurements are used. All error ranges presented account for the measurement accuracy of the equipment used, these are specified in the figure captions as appropriate.

All photographs were taken using a 3.2-s exposure time, *f*/11 aperture and a white balance of 4900 K. Flame images were captured with a Canon EOS 6D DSLR camera fitted with a 50-mm lens and 594-nm (23-nm full-width at half-maximum) notch filter. The filter is used to remove the orange colour (~589 nm) caused by sodium, attributed to impurities in the ambient air. The presence of this impurity has been documented previously [42,43] and to ensure a fair representation of the flames in this paper with others where this sodium impurity may not occur, an optical filter is used which removes the visible emissions attributed to the uncontrolled sodium in the air.

To quantify flame length, an ICCD camera is used with a 50-mm, *f*/3.5 UV lens and 310-nm bandpass filter (FWHM = 10 nm). This set up allows for the capture of chemiluminescence data of the OH* radical. The OH* species only occurs within the reaction zone of a flame, which allows for location and quantification of the flame front, separate from the ambiguity associated with traditional photography. A height above burner (HAB) scale is provided for both true-colour and OH* chemiluminescence images. Additionally, flame length is quantified from the OH* chemiluminescence data using a previously established approach [44–46]. In this case, the flame boundary layer is defined as the point at which OH* chemiluminescence intensity falls below 10 % of the peak intensity for each flame. This allows for the quantification of flame length.

Radiant heat transfer was quantified using a Medtherm heat flux sensor, fitted with a view restrictor. The view angle was restricted to 20° to isolate individual sections of the flame and provide greater spatial resolution of the heat flux profile. Axial heat flux measurements were taken using a vertical transverse, over a sampling range of 0–1200 mm HAB with a total of six sample locations. Radiant heat fraction is calculated from the axial heat flux data using Eq. (3), which is an approach adapted from previous work [47–49]. In this case, the radiant fraction (Q_r) is calculated as the sum of axial heat flux samples (Q_s) multiplied by the radiative area ($4\pi R^2$) and normalised by the total heat input from the fuel stream, given by the multiplication of lower heating value (LHV) and mass flow rate ($\dot{m}$) of the fuel. Here, R is the distance from the flame centreline to the sensor.

$$Q_r = \frac{4\pi R^2 \sum Q_{s,n}}{LHV \cdot \dot{m}} \tag{3}$$

A Teledyne gas analyser was used to collect NOx emission data. Flue gas samples were collected at 1800 mm above the burner using a capture hood. Raw data was corrected to 0 % O_2 and converted to an emission index using previously established techniques [37], shown partially in Eq. (4) where m is the mass of some pollutant (e.g. NO_2) and HHV is the higher heating value of the fuel blend.

$$EI = \frac{m}{HHV} \tag{4}$$

2.3. Flame cases

The standard operation of the AN-burner utilises natural gas, with a maximum heat input of 35 kW. In this investigation, a controlled H_2-

biogas mixture is used instead. Given biogas is composed primarily of CH_4 and CO_2, a surrogate biogas mixture composed of natural gas and CO_2 is used, as in previous investigations [19,20,22–24]. An analysis, presented in Table S1 of the Supplementary Material, showed the municipal network natural gas is approximately 97 % methane, with less than 0.4 % higher alkanes, and so has been used in place of pure CH4. Three surrogate biogas mixtures are considered, namely, BG40, BG60 and BG80 — these mixtures contain 40 %, 60 % and 80 % natural gas with the balance CO_2, with higher CH_4 contents representing higher raw biogas quality [23]. The heating values of the three surrogate biogas mixtures are 13, 20 and 27 MJ/m^3, respectively. As H_2 is added to the fuel, the flowrate of natural gas is reduced to conserve the total heat input at 35 kW. The flowrate of CO_2 is reduced in proportion to natural gas, conserving the NG/CO_2 ratio for the respective fuel blend (80/20, 60/40 or 40/60). A table of fuel compositions and related details is presented in Table 1.

Initially, H_2 is blended with each of the surrogate biogas mixtures to establish (i) the minimum H_2 fraction required to achieve combustion with each fuel blend, and (ii) the maximum H_2 fraction before flashback occurs under steady state conditions. These limits were established for all three injector sizes specified in Section 2.1. Unless otherwise specified, all H_2 fractions are calculated excluding CO_2, that is, as a percentage of fuel gases. A plot of the calculated Reynolds numbers for each fuel composition and injector size is presented in Fig. S1 in the Supplementary Material. Additionally, a table of the total volumetric percentages is presented in Table S2 in the Supplementary Material for reference.

In Section 3.1, H_2 fraction was blended in 10 vol% increments from the minimum to the maximum values which could be achieved while maintaining stable combustion for each fuel blend. Sections 3.2-3.4 presents a selected sub-set of this data, focussed primarily on the upper and lower limits of H_2 addition to each fuel blend, where the impact on the key performance criteria of the burner is investigated. The focus of this investigation is to establish the minimum and maximum H_2 fractions able/required to be blended three common fuel blends to avoid flashback or blow-off. To highlight the extremities of each fuel blend, a detailed analysis of flame appearance, NOx emission index and radiant heat transfer is provided for these maximum and minimum H_2 fractions, determined in Section 3.1. The heat input is maintained at 35 kW as fuel composition is varied. An approximate composition of the natural gas used in these experiments is outlined in Table S1 of the Supplementary Material. The H_2 and CO_2 gas used was industrial grade (assay: 99.5 % and 99.9 %, respectively) from cylinders. All gas flow rates were controlled using Alicat mass flow controllers.

3. Result and discussion

3.1. Operating range of fuel mixtures

The upper and lower fractions of H_2 able/required to be blended with three natural gas-CO_2 mixtures before flashback or blow-off are presented in Fig. 2 for three fuel injector sizes. Since H_2 fraction is varied in 10 vol% increments, error bars are given to highlight the accuracy (±10 vol% H_2) to which these limits are known.

Fig. 2 shows that for the standard (4-mm) injector size, no fraction of H_2 was found that could establish a stable BG40 flame. For the BG60 mixture, 60 and 70 vol% H_2 was required to be blended to avoid blow-off and flashback, respectively. The BG80 blend was resistant to blow off at 0 % H_2, with up to 60 vol% H_2 able to be blended before flashback occurred — 10 vol% more than for a standard natural gas mixture.

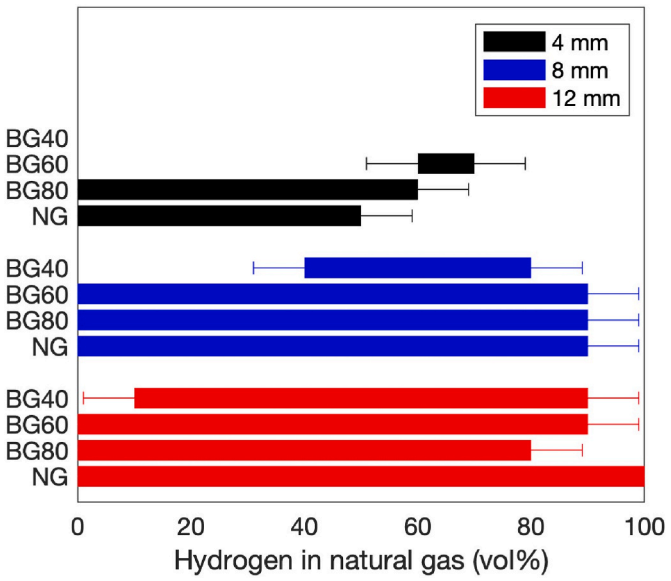

Fig. 2. Minimum and maximum fractions of hydrogen able to be blended into various natural gas (NG) and biogas (BG) fuels before blow-off or flashback while conserving heat input.

Increasing the injector size significantly widened the operating ranges for all fuel blends. By increasing the injector size to 8 mm, a BG40 mixture could be stabilised with a minimum of 40 vol% H_2 in the fuel — and flashing back at above 80 vol% H_2. BG60 and BG80 mixtures were both stable with no H_2 blending into the fuel, flashing back above 90 vol % H_2.

Further increasing the injector diameter to 12 mm allowed a BG40 mixture to resist blow-off with only 10 vol% H_2 added. The upper (flashback) limit of the BG40 blend was increased to 90 vol% H_2. The operating limits of the BG60 mixture did not change by increasing the injector diameter from 8 mm to 12 mm, however, the upper limit for H_2 addition was observed to decrease by 10 vol% for the BG80 blend. In this case, although an 80 vol% H_2 in natural gas could be established, the addition of a small amount (<5 vol% of total gas supply) of CO_2 induced a flashback event.

Because the heat input was conserved for all cases, there is an increase in total jet velocity as both H_2 and CO_2 content are increased. Consequently, it is likely that the cause for flashback in the 12 mm BG80 80 vol% flame was a result of increased primary air entrainment caused by the added fuel stream momentum as a result of the added CO_2. Fig. 3 shows calculated primary air entrainment values as a percentage of the respective fuel's stoichiometric air requirement. From Fig. 3 it can be seen that that even small amounts of H_2 or CO_2 addition, such as the added CO_2 from a high-quality biogas (i.e. BG80), caused the percentage of stoichiometric air entrained to increase from 86 % to 106 % in the 4-mm injector, making flashback more likely.

3.2. Visual observations and OH* chemiluminescence

To characterise the visual effects of fuel composition and injector size, a series of flame photographs are presented in Fig. 4.

From Fig. 4 it can be seen that the 4-mm base case (NG) flame had a consistent blue colour and a visual flame length of almost 750 mm. The BG80 gas mixture in the 4-mm injector, which required no H_2 in order to stabilise, appeared much shorter and produced two distinct regions within the flame, a bright inner core and a dim outer plume. The additional gas flow from CO_2 and/or H_2 increases the fuel stream

Table 1
Fuel composition details.

Case code	Natural Gas (vol%)	Carbon Dioxide (vol%)
NG	100	0
BG80	80	20
BG60	60	40
BG40	40	60

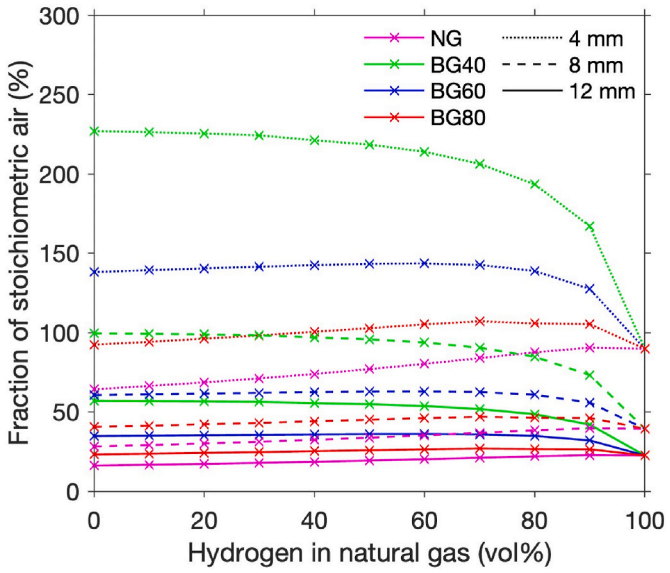

Fig. 3. Calculated primary air entrainment from Eq. (2), presented as a fraction of stoichiometric air for each fuel mixture. Solid, dashed and dotted lines represent 4-mm, 8-mm and 12-mm injector diameters, respectively.

velocity and, as highlighted in Fig. 3, increase the volume of primary air entrained. This decrease in equivalence ratio means that the reaction is less reliant on diffusion of secondary air to sustain itself, thus shortening the flame length, with such observations reported in previous work [50, 51]. For the BG80 mixture, nearly all of the stoichiometric air requirement (92 %) is entrained and so a much shorter flame length is required to complete the combustion reaction. A secondary effect is the increase or decrease in burning velocity by addition of H_2 or CO_2, respectively — the changes in burning rate caused H_2 and CO_2 has been previously linked to decreases and increases in flame length [10].

Increasing the fuel injector size decreases the fuel stream momentum, lowering the volume of primary air being entrained, and increasing equivalence ratio, as highlighted in Fig. 3. Consequently, the larger injector sizes produced flames which appeared much longer than the smaller injector flames. Increasing the injector size to 8 mm and 12 mm produced flames which appeared similar to the base (NG) case without H_2 for a BG60 and BG40 fuel mixture, respectively. As with the 4 mm injector, increasing the total gas flow via CO_2 or H_2 addition caused a shortening of the flame length and produced a second inner core in the 8 mm injector, albeit at higher flow rates compared to the 4-mm injector, suggesting the cause is related to primary air entrainment. Visually distinct flame regions have been previously documented where it was described as the result of unreacted fuel mixing with secondary air to form a second outer reaction zone [37,52–54].

A rich mixture will consume the primary air and leave unburnt or partially unburnt fuel such as carbon monoxide, since the initial fuel/air mixture was not at stoichiometric conditions and therefore cannot achieve complete combustion of the fuel. Secondary air must diffuse from the surrounding atmosphere in order to complete the reaction and hence factors such as flammability limits, differential diffusion and dilution ratio will impact this and potentially induce a second reaction zone large enough to be observed. The increased presence of H_2 will also impact this, via the preferential diffusion of H_2 — this can be observed in Fig. 4 when comparing left and right split photographs, which correspond to minimum and maximum H_2 fractions.

The 12-mm injector flames appeared more consistent across the of fuel mixtures tested, shortening only slightly. This flame shortening is likely a combination of the increased primary air entrainment, as explained above, and the effects of H_2 which often produces a shorter flame due to the increased burning rate [10]. In the 12-mm injector cases, where all three fuel mixtures could be stabilised without H_2, it can be seen that the effect of CO_2 had little impact on visibility. In contrast, H_2 addition caused a significant reduction in visibility as H_2 fraction approached 100 %. In these cases (0 % H_2 BG80 and BG60 in the 12-mm injector), the mean image intensity decreased by 8 % and 12 %, respectively, when the H_2 fraction increased to 90 vol%. To supplement the flame photographs (Fig. 3), OH* chemiluminescence images are provided in Fig. 5. These images are used to quantify flame length, which is presented in Fig. 6.

The OH* chemiluminescence flame length for the base (natural gas, 4-mm) case was 700 mm. As observed in Fig. 4, the addition of a CO_2 component in the fuel mixture caused a significant reduction in flame length, up to 78 % for the BG80 mixture.

Increasing the injector size and reducing the primary air entrainment caused an increase in flame length. For the BG80 mixture, increasing the injector size to 8 mm and 12 mm increased flame length by 6- and 6.2-times, with similar increases observed for other fuel mixtures.

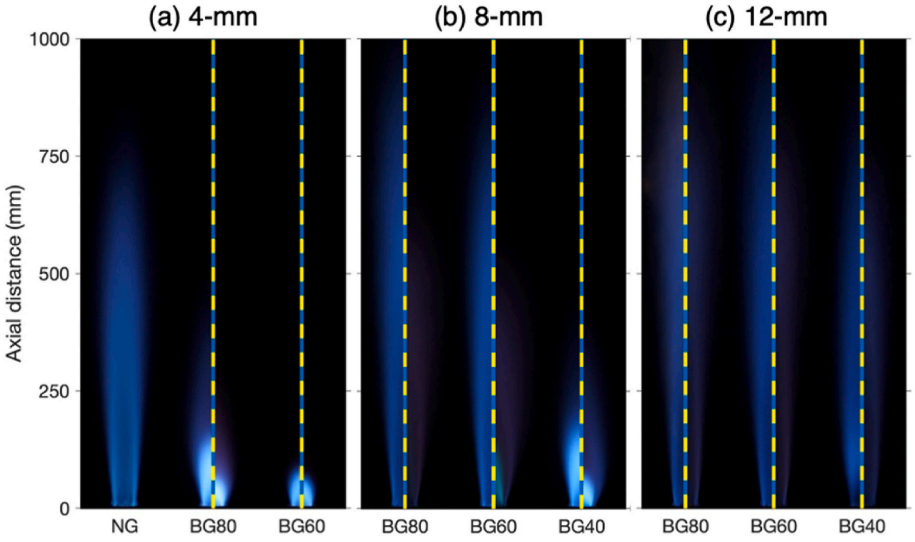

Fig. 4. True colour flame photographs of the base natural gas (NG) case flame and split photographs for hydrogen addition at the minimum (left split) and maximum (right split) volume fraction before blow-off or flashback to three fuel blends (BG80, BG60 and BG40) in a self-aspirating burner with different injector diameters: (a) 4-mm, (b) 8-mm or (c) 12-mm. All images are taken with a 594-nm notch filter at a 3.2-s exposure time, and 4900K white balance. (For interpretation of the references to colour in this figure legend, the reader is referred to the Web version of this article.)

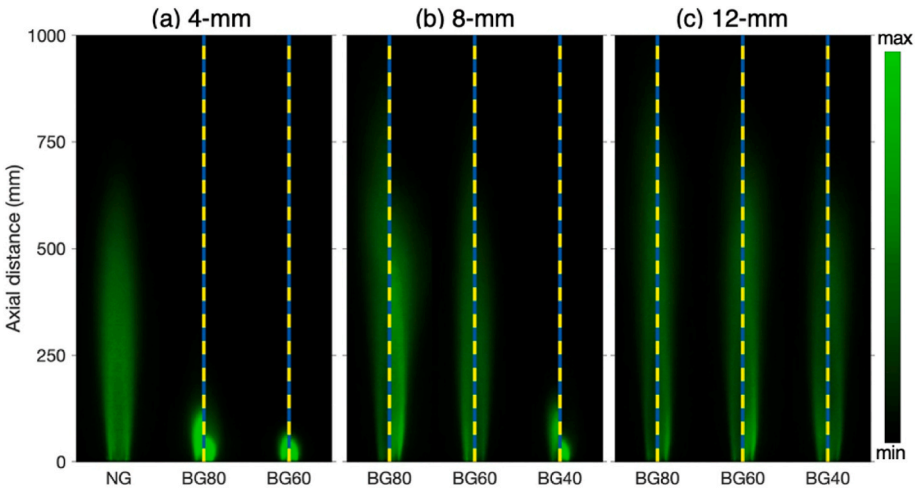

Fig. 5. False colour OH* chemiluminescence images of the base natural gas (NG) case flame and split images for hydrogen addition at the minimum (left split) and maximum (right split) volume fraction before blow-off or flashback to three fuel blends (BG80, BG60 and BG40) in a self-aspirating burner with different injector diameters: (a) 4-mm, (b) 8-mm or (c) 12-mm. All images are taken with a 310-nm bandpass filter. All images are taken with an exposure time of 2 s. Note the intensity scale for the 4-mm BG80 and BG60, and 8-mm BG40 flames is increased by a factor of four to account for the larger much larger intensity. (For interpretation of the references to colour in this figure legend, the reader is referred to the Web version of this article.)

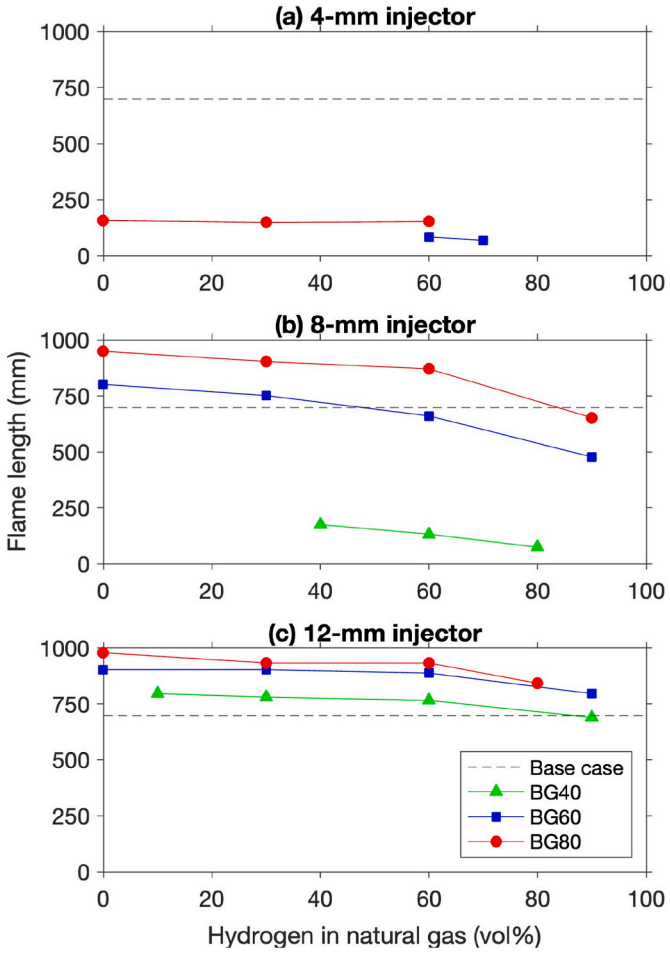

Fig. 6. Flame length (from OH* chemiluminescence images) for hydrogen addition to a natural gas (NG) or surrogate biogas (BG) mixtures in a 35 kW in a self-aspirating burner fitted with different injector diameters: (a) 4-mm, (b) 8-mm or (c) 12-mm.

The addition of H_2 causes a modest decrease in flame length up to 60 vol%, similar to previously documented trends [55]. The maximum addition of H_2 typically resulted in a decrease in flame length of ~30 % compared to the base case, depending on the CO_2 content and injector size. In combination with the larger (12-mm) injector size, the addition of 90 vol% H_2 produced a flame length equivalent to that of the base (NG) flame with the BG40 fuel mixture.

The results show the increased primary air entrainment and dilution effects as a result of adding CO_2 to the fuel stream are significant on affecting the flame length. However, the combination of H_2 addition and strategic modification of fuel injector size (or other methods to reduce primary air intake) can be used to replicate the flame appearance of the standard operation with natural gas.

3.3. *Influence of fuel composition and injector size on NOx emissions*

NOx emissions are an important metric when considering the performance of a commercial burner, especially when investigating its use with H_2. Furthermore, a potential benefit of the inert content in a H_2-biogas fuel blend is a reduced NOx emission index. Fig. 7 presents NOx emission data for each fuel mixture and injector size. Results from previous work [37] have been included as a reference to H_2-natural gas data, that is, without CO_2 addition. A separate analysis of NO and NO_2 is also provided in Fig. S2 of the Supplementary Material.

The base case, a standard (4-mm) injector, operated with the maximum nominal supply of natural gas (35 kW), produced 22 mg/MJ of NOx [37]. The addition of CO_2 in the BG80 mixture had a less than 5 % reducing effect on NOx emissions compared with the base case (21 mg/MJ). The maximum H_2 fraction for the BG80 mixture (60 vol%) produced approximately 1.5-times the NOx of the base case (33 mg/MJ). Increasing the CO_2 further (BG60) resulted in a five-fold reduction in NOx emissions for both the 60 and 70 vol% H_2 blends. In addition to a higher adiabatic flame temperature, H_2 addition is also expected to push the system closer to stoichiometric conditions due to the increased primary air entrainment and a lower stoichiometric requirement for air, compared with natural gas. Given these impacts of H_2 addition, an increase in thermal NOx emissions is expected and consistent with the observations in Fig. 7. The increased primary air entrainment as a result of CO_2 addition causes an increase in the oxidation of NO to NO_2, as shown in Fig. S2 of the Supplementary Material. This has been observed in previous work, where an increase in equivalence ratio caused a decrease in the NO_2 to NOx ratio [56]. That is, as the mixture becomes

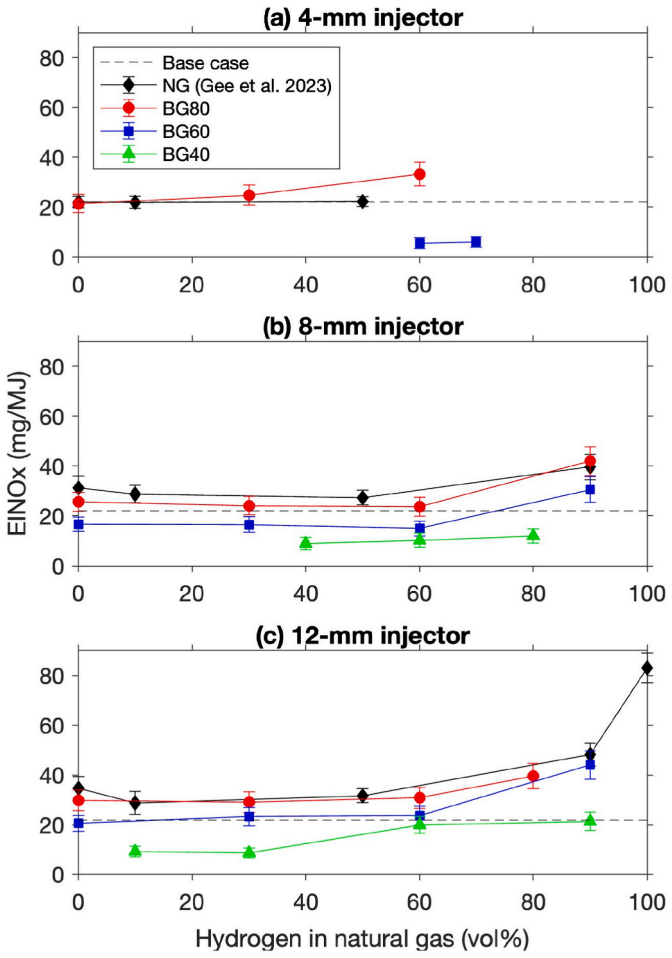

Fig. 7. NOx emission index for hydrogen addition to a natural gas (NG) or surrogate biogas (BG) mixtures in a 35 kW in a self-aspirating burner fitted with different injector diameters: (a) 4-mm, (b) 8-mm or (c) 12-mm. The error bars represent 10 % of the measured value, which is the accuracy of the measurement equipment.

richer, the conversion of NO to NO_2 is decreased. It is noteworthy that H_2 addition also increases the entrainment of primary air, albeit to a lesser extent than CO_2 for the same volume flow, which may explain why, in some cases, the conversion of NO to NO_2 increases as H_2 is added. In addition, the formation of NO is temperature dependent and although H_2 addition increases the entrainment of primary air, it may also increase flame temperature resulting in increased thermal NO formation [54,57].

When modified with the 8-mm injector, blending H_2 with the BG80 mixture had a similar impact on NOx emissions compared to natural gas. As CO_2 content increased, NOx emissions were observed to decrease. The BG60 mixture produced 33 % less NOx on average than the base BG80 mixture for the same H_2 blends. NOx emissions remained below that of the base case up to 60 vol% H_2, at 90 vol% blended into the BG60 mixture, NOx levels were 39 % higher than the base case. The BG40 mixture had the lowest NOx emissions and the narrowest operating range, producing 59 %–45 % less NOx than the base case.

The wider operating range that is achieved for the larger CO_2 dilution fuel mixtures by increasing the injector size to 12 mm, allows for operation with up to 90 vol% H_2 with NOx production equivalent to the base case. Overall, increasing the injector size further has an increasing effect on NOx emissions, for all fuel blends. It might be expected that the leaner cases (closer to $\varphi = 1$) would have a hotter flame temperature and produce higher NOx emissions, however. it is also noted that non-premixed flames also burn at $\varphi = 1$ at the reaction zone, which explains why NOx emissions increase in the cases with very high equivalence ratio [58,59]. In addition to the physical effects of CO_2 dilution, added thermal effects may have also contributed to the lack of NOx emissions, where CO_2 may have absorbed most of this heat and reradiated it, resulting in the high peak heat flux. Residence time may also be a contributing factor. Although flame temperature typically dominates the formation of thermal NOx, residence time also plays an important role. Since the flames with a high primary air entrainment are shorter, as observed in Fig. 3–6, it could be reasonably expected that the shorter residence time did not allow for a high formation of NOx.

There are two main factors which contribute to NOx formation under the present conditions, primary air entrainment and H_2 fraction, as these are variables which impact flame temperature. Previous work has shown that as primary air entrainment is decreased (via increasing the fuel injector size), NOx emissions increase, with this effect most significant at higher fractions of H_2 [37,60]. Note that this effect was observed in addition to the effects of H_2, that is, for the same fuel composition. As CO_2 content in the fuel increases, a dual effect is observed with respect to NOx emissions. As CO_2 content increases, primary air entrainment is increased due to the added fuel stream momentum, and a diluting effect is also incurred since CO_2 does not contribute to the combustion reaction.

Fuel injector diameter can be used as a tool to operate with a higher dilution of CO_2 as and/or to operate with a greater fraction of H_2, but in general should be minimised in order to maintain low NOx emissions. For example, if the goal of a specific process was to blend 90 % H_2 with BG60 mixture, this can be achieved by increasing the injector size from 4 mm to 8 mm, however, a further increase in injector size only serves to increase the NOx emissions. In reality, it is unlikely that the ultimate goal will be a specific blend ratio. It is more likely that adopters of H_2 and biogas will be looking to widen the available operating ranges, maximise H_2 addition or utilise the lowest quality of biogas. The requirements of different practical uses will vary significantly but the results presented in Fig. 7 suggest that modifying injector diameter is an effective tool to achieve a variety of targets.

3.4. Collateral impact of CO_2 dilution on radiative heat transfer

An important aspect of inert dilution research is the implications on radiant heat transfer. In this section, the collateral impact of diluting a H_2-natural gas fuel mixture with CO_2 on the radiant heat transfer capacity is presented. Fig. 8 shows the radiant fraction (refer Equation (2)) of each fuel blend and injector diameter.

The standard (4-mm) injector has a radiant fraction of 0.13 when operated with natural gas at the nominal 35 kW [37]. This is mostly unaffected when H_2 is added up to 50 vol% (the flashback limit). From Fig. 8 it can be seen that when the CO_2 is added, a reduction in radiant fraction is observed. Operation with a BG80 blend, without H_2, lowers the radiant fraction by 66 %. Addition of H_2 up to the flashback limit (60 vol% H_2) reduced the radiant fraction by 18 %. Increasing the CO_2 content further, with the BG60 mixture, caused a significant reduction — lowering radiant fraction by 66 % and 64 % compared to the base case for 60 and 70 vol% H_2 blends, respectively.

As fuel injector size increases, the difference between radiant fraction for each fuel composition decreases. In general, the effect of increasing injector size and consequently, lowering primary air entrainment, is to increase the radiant fraction of the flames. For the BG80 mixture, blended with 0, 30 and 60 vol% H_2, the radiant fraction increases by 34 % and 37 % on average for the 8-mm and 12-mm injector sizes, respectively, compared to the standard 4-mm-diameter.

Several effects work to both increased and decrease the radiant heating fraction of the fuels. As the fraction of both H_2 and CO_2 in the fuel increase, soot formation, which is the primary contributor to radiant heating capacity in hydrocarbon flames [21,29–34,61], is inhibited via multiple chemical, thermal and physical effects [35,36]. Although soot is a large contributor to radiant heat transfer, CO_2 also acts as a radiative

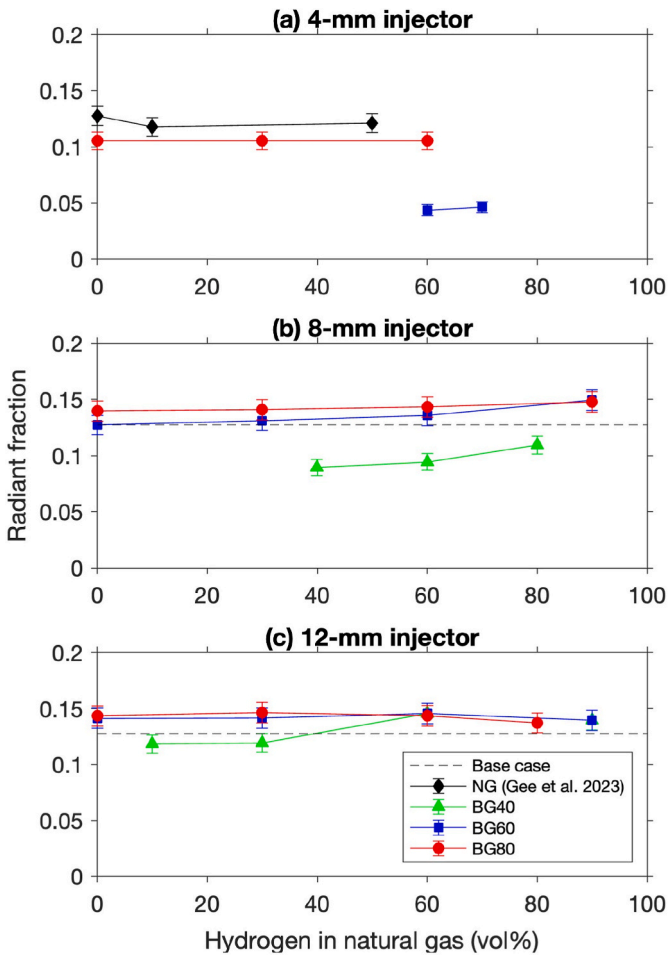

Fig. 8. Fraction of total heat transfer coming from radiation for hydrogen addition to a natural gas (NG) or surrogate biogas (BG) mixtures in a 35 kW in a self-aspirating burner fitted with different injector diameters: (a) 4-mm, (b) 8-mm or (c) 12-mm. The error bars represent 0.5 % of the measured value, which is the accuracy of the measurement equipment.

species, albeit less effectively than soot. The increased flame temperature incurred by blending with H_2 and reducing primary air intake, combined with the added radiative properties of CO_2 both work to counter the displacement of soot and maintain or increase radiant fraction.

To provide a more detailed analysis of how injector size and quality impact the radiant heat transfer properties of each flame, the axial heat flux profiles, from which the radiant fractions are calculated is presented in Fig. 9.

The axial heat flux profiles presented in Fig. 9 show that, although the total radiant fraction did not vary significantly, the axial profiles can be significantly affected. The effect of H_2 is to increase the magnitude and shift the location of peak axial heat flux, while lowering the average radiant fraction of the flames. The poor preservation of axial heat transfer properties may be significant for applications which rely on a consistent heat distribution along a known flame length to a furnace wall or other impinging point [62]. In Section 3.2 it was observed that as H_2 or CO_2 content in the fuel increases the flames become shorter and more luminous. It is also predicted in Fig. 3 that as fuel stream velocity increases, primary air intake increases. A combustion at or near stoichiometric conditions will result in high flame temperatures and consequently, high heat flux [63]. For example, H_2 addition to the BG40 blend in the 8-mm injector (subplot 'f' in Fig. 9) has a relatively high peak heat flux measurement in the initial portion of the flame but a relatively short overall radiant length. Per Fig. 3, these flames (BG40-H40-80 with 8-mm injector) entrain 75–100 % of the stoichiometric requirement for air. This high primary air entrainment shortens the flame, as observed in Fig. 4–6, and causes a strong peak in heat flux closer to the burner. Similarly, for flames which entrain greater than their stoichiometric requirement of primary air (e.g. BG60-H60-70 in the 4-mm injector), the flame becomes shorter, but the peak heat flux is relatively low compared to other cases. Additionally, the high peak heat flux for flames which use more CO_2 support the hypothesis that CO_2 is acting as a heat sink, absorbing heat and lowering thermal NOx formation (evident in Fig. 7) and reradiating thermal energy, producing the peaks nearer to the burner (evident in Fig. 9).

Although the overall radiant fractions did not vary considerably between fuel compositions and injector sizes, the high variance of the individual axial heat flux profiles warrants concern when looking to implement and/or H_2 into existing self-aspirating designs. In applications where radiant flame length is important to performance, an increase in peak radiant intensity upstream at the expense of a decrease in radiant length may be detrimental to operation, however, this appears to be partially mitigated by increasing fuel injector size and lowering the primary air entrainment. It is noteworthy that the impact of CO_2 dilution is less significant in the larger (12-mm) injector size. A good replication of the base (NG) axial heat flux profile was achieved in the larger 12-mm injector size, with increased variability between H_2 cases seen for higher CO_2 content blends. Section 3.3 showed that the increased NOx emissions caused by reducing primary air intake could be mitigated with CO_2. This suggests a middle ground can be achieved where a larger injector size expands the operating limits of each fuel mixture and reduces the collateral impact on radiant heat transfer, while the added CO_2 content maintains low NOx emissions.

4. Conclusions

A natural gas and carbon dioxide fuel mixture was enriched by hydrogen to experimentally investigate the performance of a hydrogen and surrogate biogas fuel. The performance of the various biogas qualities and hydrogen blend ratios was investigated for use in a commercial self-aspirating by quantifying the impact on primary air entrainment, blow-off and flashback limits, NOx emissions, radiant heat transfer and flame appearance. The key finding of the paper are summarised below.

1. The CO_2 content of the fuel mixtures was shown to significantly impact the stability and operation of the unmodified burner — with only high quality (low CO_2) fuel blends able to be stabilised in the standard 4-mm injector. Reducing the velocity of the fuel stream via increase fuel injector size permitted much higher CO_2 content before blowing off. The addition of H_2 also contributed to extending the blow-off limit of various fuel mixtures due to the increase burning velocity, albeit to a lesser extent than by modifying the fuel injector size. Likewise, the CO_2 content contributed to extending the flashback limit of H_2 blended fuels, again to a lesser extent than the modification of the fuel injector size.
2. The added CO_2 component caused a significant shortening of flame length (up to 78 %) due to the increased entrainment of primary air as a result of an increased axial momentum of fuel stream. Increasing the fuel injector size reduced this axial momentum component and produced longer flames with similar visibility to that of natural gas. The addition of H_2 contributed further to reductions in flame length and significantly reduced visibility.
3. The presence of CO_2 in the flames acted to reduce NOx emissions via dilution effects and an increased primary air entrainment. Increased NOx emissions as a result of H_2 blending or an increased fuel injector size were able to be mitigated with the addition of CO_2.
4. The overall radiant fractions of the flames were mostly unaffected by the CO_2 or H_2 content in the fuel. Instead, primary air intake, which is indirectly related to fuel composition in self-aspirating burners, was the most significant variable with regard to overall radiant

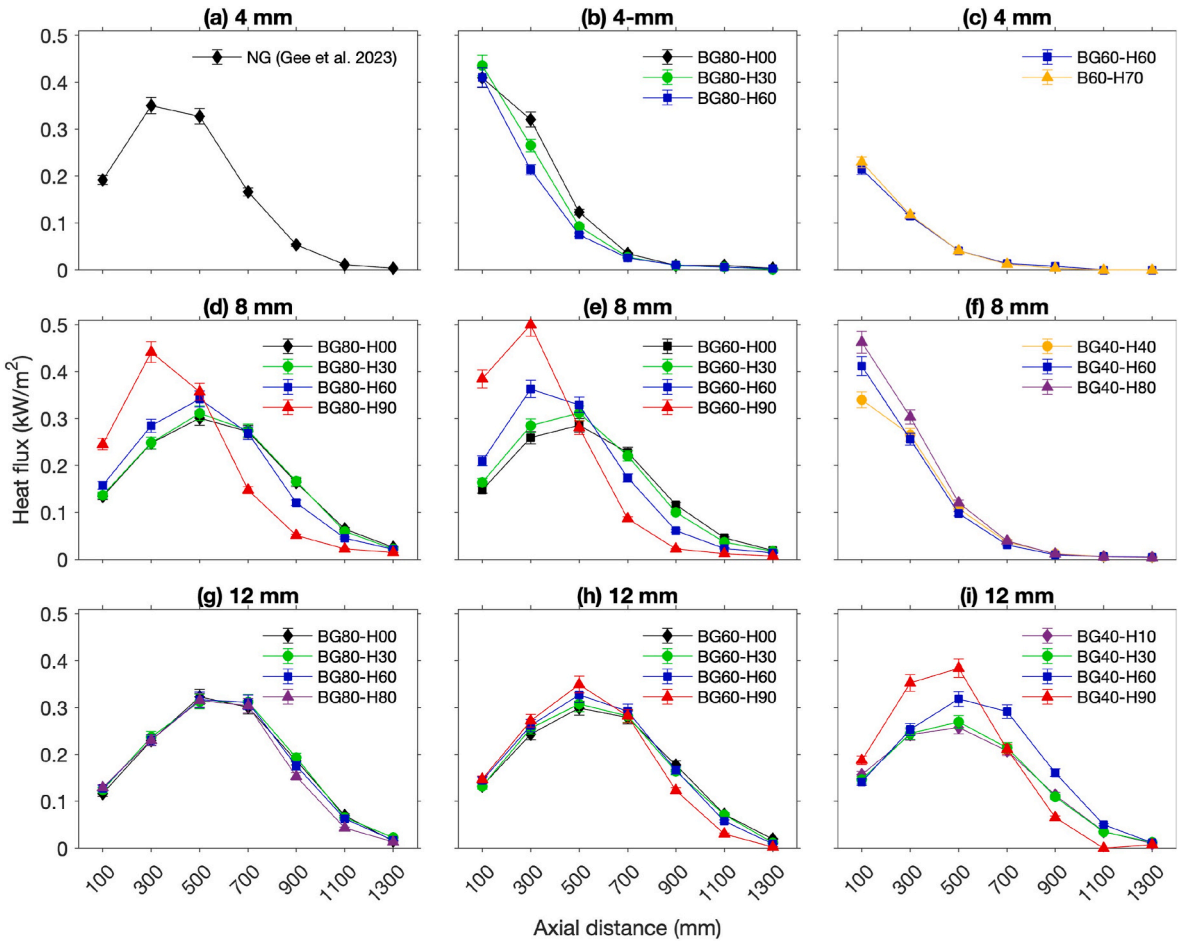

Fig. 9. Axial heat flux measurements for hydrogen addition to natural gas (NG) or surrogate (BG) mixtures in a 35 kW self-aspirating burner fitted with different injector diameters: (a, b, c) 4-mm, (d, e, f) 8-mm or (g, h, i) 12-mm. The error bars represent 0.5 % of the measured value, which is the accuracy of the measurement equipment.

fractions. Axial heat flux profiles were shown to vary significantly with CO_2, but this effect could be mitigated by increasing fuel injector size and reducing primary intake.

Declaration of competing interest

The authors declare that they have no known competing financial interests or personal relationships that could have appeared to influence the work reported in this paper.

Acknowledgements

The authors acknowledge the support from the Australian Research Council, The University of Adelaide and the Future Fuels CRC.

Appendix A. Supplementary data

Supplementary data to this article can be found online at https://doi.org/10.1016/j.ijhydene.2023.11.322.

References

[1] Giurcan V, Movileanu C, Musuc AM, Mitu M. Laminar burning velocity of biogas-containing mixtures. Literature Rev Process 2021;9(6):996. https://doi.org/10.3390/pr9060996.

[2] International Energy Agency. Outlook for biogas and biomethane. Tech Rep 2020. Available from: https://iea.blob.core.windows.net/assets/03aeb10c-c38c-4d10-bcec-de92e9ab815f/Outlook_for_biogas_and_biomethane.pdf. [Accessed 8 January 2023].

[3] Ren F, Xiang L, Chu H, Jiang H, Ya Y. Modeling study of the impact of blending N2, CO2, and H2O on characteristics of CH4 laminar premixed combustion. Energy Fuel 2020;34(2):1184–92. https://doi.org/10.1021/acs.energyfuels.9b02108.

[4] Jung C, Park J, Song S. Performance and NOx emissions of a biogas-fueled turbocharged internal combustion engine. Energy 2015:86. https://10.1016/j.energy.2015.03.122.

[5] Taleghani G, Shabani Kia A. Technical–economical analysis of the Saveh biogas power plant. Renew Energy 2005;30(3):441–6. https://doi.org/10.1016/j.renene.2004.06.004.

[6] Hosseini SE, Wahid MA. Development of biogas combustion in combined heat and power generation. Renew Sustain Energy Rev 2014;40:868–75. https://doi.org/10.1016/j.rser.2014.07.204.

[7] Acero MJ, Pacheco LE, Díaz CA. Numerical Study of the Effect of hydrogen addition on the laminar flame speed and premixed flame structure of biogas. Int J Renew Energy Resour 2018;8:1098–104.

[8] Suhaimi M, Saat A, Wahid A, Rahman M, Daierobbi G. Effect of hydrogen addition on biogas combustion and flame propagation. Jurnal Mekanikal; 2018.

[9] Acero-Caballero M, Pacheco-Sandoval L, Díaz-González C. Effect of hydrogen addition on the laminar flame speed of biogas. Experimental and numerical study. Sci Tech 2019;24:472–8.

[10] Zhen HS, Leung CW, Cheung CS. Effects of hydrogen addition on the characteristics of a biogas diffusion flame. Int J Hydrogen Energy 2013;38(16):6874–81. https://doi.org/10.1016/j.ijhydene.2013.02.046.

[11] Tabatabaei M, Aghbashlo M, Valijanian E, Kazemi Shariat Panahi H, Nizami A-S, Ghanavati H, Sulaiman A, Mirmohamadsadeghi S, Karimi K. A comprehensive review on recent biological innovations to improve biogas production, Part 1: upstream strategies. Renew Energy 2020;146:1204–20. https://doi.org/10.1016/j.renene.2019.07.037.

[12] Collins BA, Birzer CH, Harris PW, Kidd SP, McCabe BK, Medwell PR. Two-phase anaerobic digestion in leach bed reactors coupled to anaerobic filters: a review and the potential of biochar filters. Renew Sustain Energy Rev 2023;175:113187. https://doi.org/10.1016/j.rser.2023.113187.

[13] Tang S, Wang Z, Lu H, Si B, Wang C, Jiang W. Design of stage-separated anaerobic digestion: principles, applications, and prospects. Renew Sustain Energy Rev 2023;187:113702. https://doi.org/10.1016/j.rser.2023.113702.

[14] Kumar Yadav V, Ray A, Ravi MR. Experimental and computational investigation of the laminar burning velocity of hydrogen-enriched biogas. Fuel 2019;235:810–21. https://doi.org/10.1016/j.fuel.2018.08.068.

[15] Li J, Huang H, Huhetaoli Osaka Y, Bai Y, Kobayashi N, Chen Y. Combustion and heat release characteristics of biogas under hydrogen-and oxygen-enriched condition. Energies 2017;10(8):1200. https://doi.org/10.3390/en10081200.

[16] Wei Z, Zhen H, Fu J, Leung C, Cheung C, Huang Z. Experimental and numerical study on the laminar burning velocity of hydrogen enriched biogas mixture. Int J Hydrogen Energy 2019;44(39):22240–9. https://doi.org/10.1016/j.ijhydene.2019.06.097.

[17] Striūgas N, Paulauskas R, Skvorčinskienė R, Lisauskas A. Investigation of waste biogas flame stability under oxygen or hydrogen-enriched conditions. Energies 2020;13(18). https://doi.org/10.3390/en13184760.

[18] Nurmukan D, Chen TJM, Hung YM, Ismadi MZ, Chong CT, Tran MV. Enhancement of biogas/air combustion by hydrogen addition at elevated temperatures. Int J Energy Res 2020;44(3):1519–34. https://doi.org/10.1002/er.4912.

[19] Zhen HS, Leung CW, Cheung CS. A comparison of the heat transfer behaviors of biogas–H2 diffusion and premixed flames. Int J Hydrogen Energy 2014;39(2):1137–44. https://doi.org/10.1016/j.ijhydene.2013.10.100.

[20] Zhen HS, Leung CW, Cheung CS, Huang ZH. Characterization of biogas-hydrogen premixed flames using Bunsen burner. Int J Hydrogen Energy 2014;39:13292–9. https://doi.org/10.1016/j.ijhydene.2014.06.126.

[21] Gee AJ, Yin Y, Foo KK, Chinnici A, Smith N, Medwell PR. Toluene addition to turbulent H2/natural gas flames in bluff-body burners. Int J Hydrogen Energy 2022;47(65):27733–46. https://doi.org/10.1016/j.ijhydene.2022.06.154.

[22] Leung T, Wierzba I. The effect of hydrogen addition on biogas non-premixed jet flame stability in a co-flowing air stream. Int J Hydrogen Energy 2008;33:3856–62. https://doi.org/10.1016/j.ijhydene.2008.04.030.

[23] Suhaimi MS, Saat A, Wahid MA. Flammability and burning rates of low quality biogas at atmospheric condition. Jurnal Teknologi 2017;79(7–3):15–20. https://doi.org/10.11113/jt.v79.11892.

[24] Kahangamage U, Chen Y, Zhou Q, Leung CW. Can hydrogen enriched biogas be used as domestic fuel? - Part II: pollutants Emission from Combustion of Biogas/H2/air Fuel Mixture. Transactions (Hong Kong Institution of Engineers) 2021;28(2):68–74. https://doi.org/10.33430/V28N2THIE-2020-0042.

[25] Wei ZL, Leung CW, Cheung CS, Huang ZH. Effects of equivalence ratio, H2 and CO2 addition on the heat release characteristics of premixed laminar biogas-hydrogen flame. Int J Hydrogen Energy 2016;41(15):6567–80. https://doi.org/10.1016/j.ijhydene.2016.01.170.

[26] Schug KP, Manheimer-Timnat Y, Yaccarino P, Glassman I. Sooting behavior of gaseous hydrocarbon diffusion flames and the influence of additives. Combust Sci Technol 1980;22(5–6):235–50. https://doi.org/10.1080/00102208008952387.

[27] Axelbaum RL, Law CK. Soot formation and inert addition in diffusion flames. Symposium (International) on Combustion 1991;23(1):1517–23. https://doi.org/10.1016/S0082-0784(06)80421-2.

[28] Du DX, Axelbaum RL, Law CK. Soot formation in strained diffusion flames with gaseous additives. Combust Flame 1995;102(1):11–20. https://doi.org/10.1016/0010-2180(95)00043-6.

[29] Pessoa-Filho JB. Thermal radiation in combustion systems. J Braz Soc Mech Sci 1999;21(3):537–47. https://doi.org/10.1590/S0100-73861999000300014.

[30] Hamadi MB, Vervisch P, Coppalle A. Radiation properties of soot from premixed flat flame. Combust Flame 1987;68(1):57–67. https://doi.org/10.1016/0010-2180(87)90065-4.

[31] Hutny WP, Lee GK. Improved radiative heat transfer from hydrogen flames. Int J Hydrogen Energy 1991;16(1):47–53. https://doi.org/10.1016/0360-3199(91)90059-R.

[32] Saito K, Williams FA, Gordon AS. Effects of oxygen on soot formation in methane diffusion flames. Combust Sci Technol 1986;47(3–4):117–38. https://doi.org/10.1080/00102208608923869.

[33] Sen S, Puri I. Thermal radiation modeling in flames and fires. Transport Phenonema in Fires; 2008. p. 301.

[34] Schiro F, Stoppato A, Benato A. Modelling and analyzing the impact of hydrogen enriched natural gas on domestic gas boilers in a decarbonization perspective. Carbon Resour Convers 2020;3:122–9. https://doi.org/10.1016/j.crcon.2020.08.001.

[35] Gu M, Chu H, Liu F. Effects of simultaneous hydrogen enrichment and carbon dioxide dilution of fuel on soot formation in an axisymmetric coflow laminar ethylene/air diffusion flame. Combust Flame 2016;166:216–28. https://doi.org/10.1016/j.combustflame.2016.01.023.

[36] Dou Y, Liu H, Liu B, Zhang Y, Liu Y, Cheng X, Tao C. Effects of carbon dioxide addition to fuel on flame radiation fraction in propane diffusion flames. Energy 2021;218:119552. https://doi.org/10.1016/j.energy.2020.119552.

[37] Gee AJ, Proud DB, Smith N, Chinnici A, Medwell PR. Hydrogen addition to a commercial self-aspirating burner and assessment of a practical burner modification strategy to improve performance. Int J Hydrogen Energy 2023. https://doi.org/10.1016/j.ijhydene.2023.06.230.

[38] Namkhat A, Jugjai S. Primary air entrainment characteristics for a self-aspirating burner: model and experiments. Energy 2010;35(4):1701–8. https://doi.org/10.1016/j.energy.2009.12.020.

[39] Pritchard R, Guy J, Connor N. Handbook of industrial gas utilization: engineering principles and practice. United States: Van Nostrand Co; 1977.

[40] Zhao Y, McDonell V, Samuelsen S. Experimental assessment of the combustion performance of an oven burner operated on pipeline natural gas mixed with hydrogen. Int J Hydrogen Energy 2019;44(47):26049–62. https://doi.org/10.1016/j.ijhydene.2019.08.011.

[41] Jones HRN. The application of combustion principles to domestic gas burner design. Taylor & Francis; 1989.

[42] Robinson JW, Smith V. Emission spectra of organic liquids in oxy-hydrogen flames. Anal Chim Acta 1966;36:489–98. https://doi.org/10.1016/0003-2670(66)80084-3.

[43] Arens EE, Youngquist RC, Starr SO. Intensity calibrated hydrogen flame spectrum. Int J Hydrogen Energy 2014;39(17):9545–51. https://doi.org/10.1016/j.ijhydene.2014.04.043.

[44] Bergstrand P, Försth M, Denbratt I. The influence of orifice diameter on flame lift-off length. Zaragoza 2002;9:11. https://doi.org/10.1007/s12239-022-0044-8.

[45] Siebers D, Higgins B. Effects of injector conditions on the flame lift-off length of DI diesel sprays. In: Thermo-and fluid-dynamic processes in diesel engines: selected papers from the thiesel 2000 conference held in valencia, Spain; 2000. September 13–15, 2000.

[46] Xie F, Yang J, Wei J, Wu R, Song X, Wang J, Yu G. Investigation of the OH* chemiluminescence characteristics in CH4/O2 lifted flames. J Energy Inst 2021;99:31–8. https://doi.org/10.1016/j.joei.2021.08.007.

[47] Buch R, Hamins A, Konishi K, Mattingly D, Kashiwagi T. Radiative emission fraction of pool fires burning silicone fluids. Combust Flame 1997;108(1):118–26. https://doi.org/10.1016/S0010-2180(96)00098-3.

[48] Langman AS, Nathan GJ, Mi J, Ashman PJ. The influence of geometric nozzle profile on the global properties of a turbulent diffusion flame. Proc Combust Inst 2007;31(1):1599–607. https://doi.org/10.1016/j.proci.2006.07.165.

[49] Dong X, Nathan GJ, Mahmoud S, Ashman PJ, Gu D, Dally BB. Global characteristics of non-premixed jet flames of hydrogen–hydrocarbon blended fuels. Combust Flame 2015;162(4):1326–35. https://doi.org/10.1016/j.combustflame.2014.11.001.

[50] Kim M, Oh J, Yoon Y. Flame length scaling in a non-premixed turbulent diluted hydrogen jet with coaxial air. Fuel 2011;90(8):2624–9. https://doi.org/10.1016/j.fuel.2011.03.036.

[51] Gupta AK, Bolz S, Hasegawa T. Effect of air preheat temperature and oxygen concentration on flame structure and emission. J Energy Resour Technol 1999;121(3):209–16. https://doi.org/10.1115/1.2795984.

[52] Schefer RW, Kulatilaka WD, Patterson BD, Settersten TB. Visible emission of hydrogen flames. Combust Flame 2009;156(6):1234–41. https://doi.org/10.1016/j.combustflame.2009.01.011.

[53] Design of gas burners for domestic use. In: Commerce Do, editor. Letter circular No. 299. Washington DC: Bureau of Standards; 1931.

[54] Naha S, Aggarwal SK. Fuel effects on NOx emissions in partially premixed flames. Combust Flame 2004;139(1):90–105. https://doi.org/10.1016/j.combustflame.2004.07.006.

[55] Wu L, Kobayashi N, Li Z, Huang H, Li J. Emission and heat transfer characteristics of methane–hydrogen hybrid fuel laminar diffusion flame. Int J Hydrogen Energy 2015;40(30):9579–89. https://doi.org/10.1016/j.ijhydene.2015.05.096.

[56] Shudo T, Omori K, Hiyama O. Emission characteristics of NO and NO2 in rich-lean combustion of hydrogen. In: ASME 2003 international mechanical engineering congress and exposition; 2003.

[57] Naha S, Briones AM, Aggarwal SK. Effect of fuel blends on pollutant emissions in flames. Combust Sci Technol 2004;177(1):183–220. https://doi.org/10.1080/00102200590883822.

[58] Law CK, Makino A, Lu TF. On the off-stoichiometric peaking of adiabatic flame temperature. Combust Flame 2006;145(4):808–19. https://doi.org/10.1016/j.combustflame.2006.01.009.

[59] Ashrafi ZN, Ashjaee M, Askari M. Two-dimensional temperature field measurement of a premixed methane/air flame using Mach–Zehnder interferometry. Opt Commun 2015;341:55–63.

[60] Shchepakina EA, Zubrilin IA, Kuznetsov AY, Tsapenkov KD, Antonov DV, Strizhak PA, Yakushkin DV, Ulitichev AG, Dolinskiy VA, Hernandez Morales M. Physical and chemical features of hydrogen combustion and their influence on the characteristics of gas turbine combustion chambers. Appl Sci 2023;13(6):3754. https://doi.org/10.3390/app13063754.

[61] Wang Y, Gu M, Zhu Y, Cao L, Zhu B, Wu J, Lin Y, Huang X. A review of the effects of hydrogen, carbon dioxide, and water vapor addition on soot formation in hydrocarbon flames. Int J Hydrogen Energy 2021;46(61):31400–27. https://doi.org/10.1016/j.ijhydene.2021.07.011.

[62] Raj VC, Kuntikana P, Sreedhara S, Prabhu SV. Separation of heat transfer components from impinging methane diffusion flames. Int J Heat Mass Tran 2018;126:123–38. https://doi.org/10.1016/j.ijheatmasstransfer.2018.05.014.

[63] Ma Q, Zhang Q, Chen J, Huang Y, Shi Y. Effects of hydrogen on combustion characteristics of methane in air. Int J Hydrogen Energy 2014;39(21):11291–8. https://doi.org/10.1016/j.ijhydene.2014.05.030.